

POLARIZED FLUORESCENCE PHOTOBLEACHING RECOVERY FOR MEASURING ROTATIONAL DIFFUSION IN SOLUTIONS AND MEMBRANES

MARISELA VELEZ AND DANIEL AXELROD

*Biophysics Research Division and Department of Physics, University of Michigan, Ann Arbor,
Michigan 48109*

ABSTRACT A variation of fluorescence photobleaching recovery (FPR) suitable for measuring the rate of rotational molecular diffusion in solution and cell membranes is presented in theory and experimental practice for epi-illumination microscopy. In this technique, a brief flash of polarized laser light creates an anisotropic distribution of unbleached fluorophores which relaxes by rotational diffusion, leading to a time-dependent postbleach fluorescence. Polarized FPR (PFPR) is applicable to any time scales from seconds to microseconds. However, at fast (microsecond) time scales, a partial recovery independent of molecular orientation tends to obscure rotational effects. The theory here presents a method for overcoming this reversible photobleaching, and includes explicit results for practical geometries, fast wobble of fluorophores, and arbitrary bleaching depth. This variation of a polarized luminescence "pump-and-probe" technique is compared with prior ones and with "pump-only" time-resolved luminescence anisotropy decay methods. The technique is experimentally verified on small latex beads with a variety of diameters, common fluorophore labels, and solvent viscosities. Preliminary measurements on a protein (acetylcholine receptor) in the membrane of nondeoxygenated cells in live culture (rat myotubes) show a difference in rotational diffusion between clustered and nonclustered receptors. In most experiments, signal averaging, high laser power, and automated sample translation must be employed to achieve adequate statistical accuracy.

INTRODUCTION

Diffusive motion of polymers and membrane components has been extensively studied in the last decade because of the information it provides about molecular size, shape, aggregation, kinetics, biological function, and intermolecular bonding.

Translational ("lateral") diffusion is directly important because it often determines the kinetic rate of certain chemical reactions (Axelrod, 1983). Translational diffusion on membranes and cell surfaces has been most often measured by variations of the fluorescence photobleaching recovery (FPR) technique (Axelrod et al, 1976*a*; also called fluorescence recovery after photobleaching [FRAP] or fluorescence microphotolysis [FM]).

Rotational diffusion is likewise interesting because it is more sensitive to molecular size and shape than translational diffusion and can be used as an indicator of changes in those features. For time scales between 1 ns and 1 μ s, rotational diffusion has been measured by optical techniques including time-resolved or phase-shift fluorescence anisotropy decay. For time scales more appropriate to membranes and cells, time-resolved phosphorescence anisotropy decay (TPA) or fluorescence depletion anisotropy (FDA) have been employed. These two latter techniques, although sensitive, have some limitations. (a) They require

deoxygenated samples, somewhat incompatible with living cell cultures, to lengthen the triplet state lifetimes upon which they depend. (b) Their time scales are limited to $< \sim 1$ ms, which is too short to measure the rotational diffusion of certain cell surface receptors. (c) The choice of triple probes is somewhat narrow (although several popular fluorophores do exhibit phosphorescence upon deoxygenation).

An alternative is to apply FPR to rotational diffusion by deliberately photobleaching with brief pulse of polarized light. The photobleaching-induced anisotropic orientational distribution of unbleached fluorophore then relaxes by diffusion back toward greater isotropicity. This relaxation is then "probed" by a much attenuated polarized beam that excites fluorescence observed through a microscope polarizer. Although conceptually similar to standard FPR, polarized FPR (PFPR) requires a much faster data acquisition rate in a microsecond range appropriate for rotational diffusion.

PFPR has been investigated by several groups in the last few years. Smith et al. (1981) introduce the technique with a theory appropriate for epifluorescence microscope geometry (observation by a finite aperture objective along the optical axis of the excitation beam) in only the weak bleaching limit for isotropic rotational diffusion in two or three dimensions. Smith et al. apply the theory to experi-

mental verification, although on systems with very long rotational times (tenths of seconds). Wegener and Rigler (1984) and Wegener (1984) present an elegant theory in very general form and reduce it to specific solutions for the nonmicroscope case in which the observation axis is orthogonal to the excitation beam axis. They find "magic" experimental configurations in which the results reflect only translational diffusion or in which the rotationally dependent results assume a particularly simple form. (Unfortunately, a standard epi-illumination microscope geometry is not such a "magic" configuration). Dale (1987) further develops the theory for isolating translational information from a process that also contains rotation on the same time scale.

PFPR is basically a generalization of fluorescence depletion anisotropy (FDA) which extends its use to any time scale longer than milliseconds for studies in single living cells in aerobic cultures. FDA was first introduced by Johnson and Garland (1981, 1982). Yoshida and Barisas (1986) present a theory for FDA which we compare with this extension in some detail later.

In this paper, we present a theory and experimental demonstration of PFPR that is especially suitable for microscopes. The theory offers an exact explicit form for the rotationally dependent part of the recovery curves for arbitrary bleaching depth and for fluorophores undergoing restricted fast wobbling at the covalent bond of attachment. The theory includes a method for eliminating the effects of fluorescence recoveries arising from ubiquitous rotation-independent phenomena. Two practical cases are considered: two-dimensional diffusion around a membrane normal presumed parallel to the optical axis; and three-dimensional isotropic diffusion. The formalism is easily generalizable to other more complex diffusive motions.

The experimental demonstration shows that sample times as short as 5 μ s may be used to gather data with characteristic times in the tenths-of-millisecond range with sufficient accuracy within a reasonable experimental time. The main source of noise arises from photon statistics. In principle, sample times down to ~ 1 μ s could be utilized with marginally acceptable accuracy and feasible experimental times on samples with characteristic times in the tens of microseconds.

This paper presents the first direct test of a polarized "pump-and-probe" fluorescence technique on well-defined spherical latex bead samples. Previous experimental checks were limited to proteins of uncertain effective hydrodynamic radius (Johnson and Garland, 1982; Yoshida and Barisas, 1986) or lipid systems of uncertain fluidity (Smith et al, 1981). We present data on model systems of varying particle size, solvent viscosity, and fluorophore type; the data is fit to the described theory; and the results for the rotational diffusion coefficient D are compared with the predictions of hydrodynamics. We also present preliminary data applying polarized FPR to measure D of an *in vivo* membrane protein, the acetylcholine

receptor (AChR) in rat myotubes in living primary culture.

PFPR and FDA are "pump-and-probe" techniques in which a flash of bleaching light (the "pump") induces an anisotropy of unbleached luminophore in the sample and an attenuated excitation beam "probes" the subsequent reorientations without inducing significant further bleaching. TPA, on the other hand, is a "pump-only" technique in which the postflash signal arises directly from delayed luminescence without further excitation. Although mathematically distinct from PFPR and applicable only to time ranges < 1 ms, TPA has yielded much important information about rotational diffusion of cell surface components. Theoretical work relevant to TPA has been presented by many groups, including Kinoshita et al. (1977, 1984) and Szabo (1984), and experimental TPA results on fast rotations of AChR have been presented by Lo et al. (1980) and by Bartholdi et al. (1981).

An experimental paper utilizing the theory and experimental apparatus for PFPR detailed here as applied to reorientational motions in DNA, has already appeared (Scalettar et al., 1988).

THEORY

General Considerations

We assume that the system consists of dipoles undergoing isotropic rotational diffusion in two or three dimensions. We assume that the characteristic diffusion time is slow compared to the bleach pulse duration, so that very little motion occurs during the bleaching pulse. Later, we will allow for a superimposed motion that is very fast compared with both the bleaching duration and the fluorescence lifetime, a motion that is called "fast wobbling."

Consider a coordinate system with absorption and emission dipoles denoted by unit vectors $\hat{\mu}_a$ and $\hat{\mu}_e$ at the origin. Because the bleaching flash is at the same wavelength as the excitation probe beam, we assume the dipole relevant for bleaching is parallel to $\hat{\mu}_a$. For many common fluorescent probes (including rhodamine, fluorescein, parinaric acid, diphenylhexatriene, eosin, erythrosin, and carbocyanine), the angle between $\hat{\mu}_a$ and $\hat{\mu}_e$ is practically zero (based on steady-state anisotropy in samples with restricted mobility; see Jameson et al. [1978]; Yoshida and Barisas [1987]; Axelrod [1979]; Dr. David Jameson, private communication). Nevertheless, we assume an arbitrary interdipole angle χ for maximum generality.

The microscope's optical axis is the x -axis; the y - and z -axes lie in the plane of the microscope stage, with the z -axis along the polarization direction of the laser "probe" beam. The emission (as gathered by microscope epi-illumination optics) is observed through a polarizing filter oriented to pass only light polarized along the z -axis. The emission polarizer is not essential for polarized FPR in principle, but as applied to microscopy in practice, the

filter is essential to circumvent the unpredictable partial polarization bias arising from the internal mirrors and filters of the particular microscope employed. Omitting the emission polarizer should not increase the quality of the results substantially because the additional y -polarized emission that would be transmitted is not optimally excited by the z -polarized probe beam.

Two polarization modes (denoted \parallel and \perp) are used. These modes are distinguished only by the polarization direction of the incident beam during the bright bleaching pulse: along the z -axis for \parallel mode and along the x -axis for \perp mode. For both modes during the pre- and postbleach phases of the experiment, the incident beam is always polarized along z .

The \parallel mode fluorescence $F_{\parallel}(t)$ after a bleaching pulse at $t = 0$ is:

$$F_{\parallel}(t) = \int (\hat{\mu}_a \cdot \hat{z})^2 (\hat{\mu}_e \cdot \hat{z})^2 C(\Omega, t) d\Omega, \quad (1)$$

where $(\hat{\mu}_a \cdot \hat{z})^2$ arises from the probability of absorption of z -polarized incident light and $(\hat{\mu}_e \cdot \hat{z})^2$ arises from the probability of emission with a polarization along z . $C(\Omega, t)$ is the concentration of unbleached fluorophore absorption dipoles at time t at generalized angle Ω (to be defined later according to the geometry and dimensionality), normalized so that the prebleach concentration $C(\Omega, -) = 1$. (The minus sign in the argument refers to times $t < 0$.) All constant factors involving efficiencies of absorption, emission, and collection that simply multiply the integral of Eq. 1 have been suppressed.

The integration over Ω in Eq. 1 also symbolically implies an average over all emission dipole angles corresponding to each absorption dipole, given the interdipole angle χ . That average can be performed immediately, yielding a substitution of $(\hat{\mu}_e \cdot \hat{z})^2$ with $(\hat{\mu}_a \cdot \hat{z})^2 (3\cos^2\chi - 1)/2 + (\sin^2\chi)/2$.

The expression for $F_{\perp}(t)$, for which the bleaching polarization is along the y -axis rather than the z -axis, would be similar to Eq. 1 except with $C(\Omega, t)$ replaced by some other concentration function reflecting an initial condition rotated by 90° . It is mathematically more convenient, however, to preserve the $C(\Omega, t)$ factor as is, and instead account for the \perp bleaching within the factors involving $\hat{\mu}_{a,e}$. Note that bleaching along y coupled with a probe excitation and emission polarization along z should yield exactly the same fluorescence as bleaching along z coupled with probe excitation and emission polarization along y . Therefore,

$$F_{\perp}(t) = \int (\hat{\mu}_a \cdot \hat{y})^2 (\hat{\mu}_e \cdot \hat{y})^2 C(\Omega, t) d\Omega. \quad (2)$$

The interdipole angle averaging can be handled in exactly the same manner as just described.

The normalized concentration of bleached (rather than unbleached) fluorophore, $\Delta C(\Omega, t) \equiv 1 - C(\Omega, t)$, is likewise related to the difference $\Delta F \equiv F(-) - F(t)$ between

the postbleach and prebleach fluorescence:

$$\Delta F_{\parallel}(t) = \int (\hat{\mu}_a \cdot \hat{z})^2 (\hat{\mu}_e \cdot \hat{z})^2 \Delta C(\Omega, t) d\Omega, \quad (3)$$

$$\Delta F_{\perp}(t) = \int (\hat{\mu}_a \cdot \hat{y})^2 (\hat{\mu}_e \cdot \hat{y})^2 \Delta C(\Omega, t) d\Omega. \quad (4)$$

In view of Eqs. 3 and 4, one can view ΔF as the "signal" that arises from the projection of bleached fluorophore dipoles along the z or y axes.

Reversible Photobleaching

An unexpected phenomenon in fast polarized FPR greatly affects experimental results: reversible photobleaching. We find that rhodamine, fluorescein, and carbocyanine fluorophores, in a variety of environments, always exhibit a partial fluorescence recovery after photobleaching independent of polarization, bleach intensity, or bleach duration. This reversible photobleaching occurs on the fast time scale of hundreds of microseconds, and for this reason has not been reported previously at the much slower time scales of standard FPR employed for measuring translational diffusion or surface chemical kinetics.

The effect of reversible photobleaching is treated theoretically here by assuming that a bleached fluorophore has an average characteristic rate α by which it returns to the unbleached state. In general, rate α may depend on the type of bleached state or the local environment of each fluorophore. Chemically identical fluorophores in a sample may exhibit a wide range of intrinsic recovery rates after reversible photobleaching, with some (the irreversibly photobleached ones) not recovering at all. The total bleached concentration $\Delta C(\Omega, t)$ is then an integral over the bleached concentration of each fluorophore $\Delta C_{\alpha}(\Omega, t)$ with its own distinct constant α :

$$\Delta C(\Omega, t) = \int \Delta C_{\alpha}(\Omega, t) d\alpha. \quad (5)$$

Each $\Delta C_{\alpha}(\Omega, t)$ has an initial condition of the same form as the others but obeys a diffusion equation with a decay term with its own factor α :

$$\frac{\partial \Delta C_{\alpha}(\Omega, t)}{\partial t} = \nabla^2 \Delta C_{\alpha}(\Omega, t) - \alpha \Delta C_{\alpha}(\Omega, t). \quad (6)$$

The general solution of Eq. 6 is simply

$$\Delta C_{\alpha}(\Omega, t) = \Delta C_{\alpha} e^{-\alpha t} \cdot \Delta C'(\Omega, t), \quad (7)$$

where $\Delta C'(\Omega, t)$ is the solution of the diffusion equation without the decay term and ΔC_{α} is a constant proportional to the relative total amount of the bleached species with decay rate α .

Combining Eq. 7 with Eq. 5 gives

$$\Delta C(\Omega, t) = \alpha(t) \cdot \Delta C'(\Omega, t), \quad (8)$$

where $\alpha(t)$, an integral over all the $e^{-\alpha t}$ terms multiplied by their own ΔC_{α} relative weights, is the total decay function

of all the bleached fluorophores. Function $\alpha(t)$ is generally nonexponential and approaches a nonzero asymptote as $t \rightarrow \infty$, corresponding to the irreversible bleaching component seen in standard slow FPR.

Function $\alpha(t)$ dominates the fluorescence recoveries and tends to obscure the rotational diffusion information contained in $\Delta C'(\Omega, t)$. However, Eqs. 3, 4, and 8 show that $\alpha(t)$ cancels from a ratio

$$R(t) = \Delta F_{\perp}(t)/\Delta F_{\parallel}(t). \quad (9)$$

For this reason, data is always taken in both \parallel and \perp mode for every experiment and the results expressed in terms of the ratio $R(t)$ or functions of $R(t)$. $R(t)$ is generally less than unity, increases with t , and approaches unity for long t . Physically, this behavior arises from the effectively shallower bleach in the \perp mode (in which those fluorophores in the best-observed orientations are not the most heavily bleached ones), and the randomizing effect of diffusion which allows the sample to "forget" in which orientation it had been bleached.

A more familiar-looking ratio reminiscent of the time-resolved fluorescence or phosphorescence anisotropy $r(t)$, is $r_b(t)$ (where the subscript stands for "bleaching"):

$$r_b(t) = \frac{1 - R(t)}{1 + 2R(t)}. \quad (10)$$

The amplitude of anisotropy $r_b(t)$ is affected by the interdipole angle, but it always remains positive and monotonically decreasing in t , regardless of the interdipole angle χ . That feature, among others discussed later, distinguishes $r_b(t)$ from the more familiar "pump-only" $r(t)$, the sign and trend of which does depend on the interdipole angle.

Initial Condition

$\Delta C'(\Omega, t)$ can be written as an integral involving the actual initial condition $\Delta C'(\Omega_0, t)$ and the diffusion equation solution for a δ -function initial condition (i.e., the Green's function G):

$$\Delta C'(\Omega, t) = \int \Delta C'(\Omega_0, 0)G(\Omega, \Omega_0, t) d\Omega_0 \quad (11)$$

Assuming that the bleaching pulse is short compared with any sample motions and that the probability rate of bleaching is proportional to the light absorbed by the fluorophore, then

$$\Delta C'(\Omega_0, 0) = 1 - \exp[-B(\hat{\mu}_{a_0} \cdot \hat{z})^2], \quad (12)$$

where B is a "bleaching parameter" for polarized FPR and is proportional to the product of bleaching light intensity, duration, absorption coefficient, and bleaching efficiency. As discussed by Dale (1987), $B = 2K$, where K is the more familiar bleaching coefficient for translational FPR in which the bleaching pulse duration is much longer than the rotational diffusion characteristic times. For shallow

bleaches,

$$\lim_{B \rightarrow 0} \Delta C'(\Omega_0, 0) \approx B(\hat{\mu}_{a_0} \cdot \hat{z})^2. \quad (13)$$

Green's Functions

The Green's functions $G(\Omega, \Omega_0, t)$ for two- and three-dimensional rotational diffusion are "well known" and can be derived easily by separating variables and forming linear combinations of general solutions with multiplicative factors that both fit the periodic boundary conditions and a δ -function initial condition.

In two dimensions with cylindrical coordinate $\Omega \equiv \theta$,

$$G(\Omega, \Omega_0, t) = \pi^{-1} \sum_{n=0}^{\infty} \left(\frac{\delta_{n0}}{2} + \cos n\Delta\theta \right) e^{-n^2 D t}, \quad (14)$$

where $\Delta\theta \equiv \theta - \theta_0$ and δ_{n0} is a Kronecker delta.

Because $\cos n\Delta\theta = \cos n\theta_0 \cos n\theta + \sin n\theta \sin n\theta_0$, the integrations over θ and θ_0 called for in Eqs. 3, 4, and 11 can be performed separately, and only the $n = 0, 2$, and 4 terms in the sum of Eq. 14 survive.

In three dimensions with spherical coordinates $\Omega \equiv (\theta, \phi)$ and azimuthal symmetry around each $\hat{\mu}_{a_0}$ (expected for isotropic diffusion),

$$G(\Omega, \Omega_0, t) = \sum_{n=0}^{\infty} \frac{2n+1}{2} P_n(\cos \Delta\theta) e^{-n(n+1) D t}, \quad (15)$$

where $\Delta\theta \equiv \theta - \theta_0$ and $P_n(\cos \Delta\theta)$ is a Legendre polynomial. As expected, there is no dependence on $\Delta\phi \equiv \phi - \phi_0$. Eq. 14 can be expressed in terms of Ω and Ω_0 variables by using the addition rule for spherical harmonics (Jackson, 1975), analogous to the trigonometric identity used above for 2-D diffusion:

$$P_n(\cos \Delta\theta) = P_n(\cos \theta) P_n(\cos \theta_0) + 2 \sum_{m=1}^n \frac{(n-m)!}{(n+m)!} P_n^m(\cos \theta) P_n^m(\cos \theta_0) \cos m\Delta\phi, \quad (16)$$

where $P_n^m(\cos \theta)$ is an associated Legendre polynomial. Upon integration over θ_0 , the summation term in Eq. 16 drops out, leaving integrals that are separable in θ and θ_0 . As for the 2-D case, only the $n = 0, 2$, and 4 terms survive.

Wobbling

Fluorophores bound to macromolecules through a single bond are likely to rotationally diffuse rapidly within a cone around some mean orientation. However, the effect of this motion upon fluorescence polarization is far from simple. Affected by steric hinderances and bond-bending energies, wobbling within the "cone" may not be symmetrical, and each angle within the cone may not be accessed with equal probability. Furthermore, the speed of such wobbling will determine how far an excited fluorophore can reorient itself before it emits.

For "pump-only" techniques, wobbling has been handled theoretically by Szabo (1984) and Kinoshita et al. (1977, 1984). For "pump-and-probe" methods, a formalism for handling wobbling has been presented by Wegener (1984) and by Scalettar et al. (1988) under the assumptions that the fluorophore is equally likely to assume any angle within a symmetrical hard cone of semiangle ψ_0 , and that the wobbling is fast compared with the fluorescence lifetime.

We generalize the geometry of those previous calculations here by allowing the azimuthally symmetric cone to be hollow, ranging in polar angle from ψ_1 to ψ_2 . (A hollow cone would result, for example, from a fluorophore free to azimuthally revolve around a molecular bond whose pointing direction is nonparallel to the dipole.) With reference to our particular geometry, one can replace each vectorial dot product term involving $\hat{\mu}_a$ or $\hat{\mu}_{a0}$ with a corresponding dot product averaged over the solid angle contained within the cone, where the original $\hat{\mu}_a$ or $\hat{\mu}_{a0}$ become the directions of the cone axes of revolution. For example,

$$(\hat{\mu}_a \cdot \hat{z})^2 \rightarrow \langle (\hat{\mu}'_a \cdot \hat{z})^2 \rangle \equiv N^{-1} \int (\hat{\mu}'_a \cdot \hat{z})^2 \sin \psi \, d\psi \, d\omega, \quad (17)$$

and likewise for $(\hat{\mu}_a \cdot \hat{y})^2$. Unit vector $\hat{\mu}'_a$ refers to the instantaneous position of the absorption dipole in the cone, which is a function of both cone azimuthal angle ω (to be integrated from $0 \rightarrow 2\pi$) and cone polar angle ψ (to be integrated from $\psi_1 \rightarrow \psi_2$), and normalization $N(\psi_1, \psi_2) \equiv \int \sin \psi \, d\psi \, d\omega$. After using the solid geometry rule for the cosine of the angle between two lines, we deduce a substitution of $(\hat{\mu}'_a \cdot \hat{z})^2$ with the linear combination $(\hat{\mu}_a \cdot \hat{z})^2 X_1 + X_2$, and likewise for $(\hat{\mu}_a \cdot \hat{y})^2$, where X_1 and X_2 are complicated constants involving only ψ_1 and ψ_2 .

Recall that the previous averaging over the squares of the emission dipole components also yielded a linear combination substitution. Taking both the wobbling and interdipole angle linear combinations into account, we obtain certain factors which will appear in the final results:

$$\begin{aligned} Z_1 &\equiv X_1^2 Y_1 \\ Z_2 &\equiv X_1 X_2 Y_1 + X_1 Y_2 / 2 \\ Z_3 &\equiv X_2^2 Y_1 + X_2 Y_2, \end{aligned} \quad (18)$$

where

$$\begin{aligned} X_1 &\equiv [(\cos^3 \psi_1 - \cos^3 \psi_2) \\ &\quad - (\cos \psi_1 - \cos \psi_2)] / 2 (\cos \psi_1 - \cos \psi_2) \\ X_2 &\equiv \left[-\frac{1}{3} (\cos^3 \psi_1 - \cos^3 \psi_2) \right. \\ &\quad \left. + (\cos \psi_1 - \cos \psi_2) \right] / 2 (\cos \psi_1 - \cos \psi_2) \\ Y_1 &\equiv (3 \cos^2 \chi - 1) / 2 \\ Y_2 &\equiv (\sin^2 \chi) / 2. \end{aligned} \quad (19)$$

If the fluorophore does not wobble, then $X_1 = 1$ and $X_2 = 0$. In most cases of interest, $\chi = 0$ and therefore $Y_1 = 1$ and $Y_2 = 0$.

We are now in a position to calculate $\Delta F_{\parallel}(t)$ and $\Delta F_{\perp}(t)$. The algebra indicated by Eqs. 1–19 is tedious but straightforward; the results for $\Delta F_{\parallel,\perp}(t)$ from which ratios $R(t)$ and $r_b(t)$ can be formed are as follows.

Final Expressions: Two Dimensions

Rotational diffusion in two dimensions is expected for membrane lipids or proteins about an axis normal to the membrane. We assume here that this axis of rotation is fixed in orientation.

$$\begin{aligned} \Delta F_{\perp}(t) &= a - b e^{-4Dt} - c e^{-16Dt} \\ \Delta F_{\parallel}(t) &= a + b e^{-4Dt} - c e^{-16Dt}, \end{aligned} \quad (20)$$

where

$$a \equiv 1 - \eta g_0 \quad (21)$$

$$b \equiv \frac{4}{3} \eta g_2 \left(\frac{Z_1 \cos^4 \epsilon + 2Z_2 \cos^2 \epsilon}{Z_1 \cos^4 \epsilon + \frac{8}{3} Z_2 \cos^2 \epsilon + \frac{8}{3} Z_3} \right) \quad (22)$$

$$c \equiv \frac{1}{3} \eta g_4 \left(\frac{Z_1 \cos^4 \epsilon}{Z_1 \cos^4 \epsilon + \frac{8}{3} Z_2 \cos^2 \epsilon + \frac{8}{3} Z_3} \right), \quad (23)$$

where

$$\eta \equiv \exp(-BX_2) \quad (24)$$

Angle ϵ is the (fixed) "tilt" angle between the dipole and the two-dimensional plane. This angle appears above only in the terms involving wobble and interdipole angles; if wobbling does not occur (i.e., $X_1 = 1$ and $X_2 = 0$) and $\chi = 0$, then the ϵ dependence disappears.

The two-dimensional g_l are products of an exponential and a modified Bessel function $I_{l/2}$ (Abramowitz and Stegun, 1965, section 9.6) with arguments involving the wobble angles, the bleaching depth B , and fixed angle ϵ as follows:

$$g_l \equiv e^{-B'} I_{l/2}(B'), \quad (25)$$

where

$$B' \equiv \frac{1}{2} B X_1 \cos^2 \epsilon. \quad (26)$$

Final Expressions: Three Dimensions

Rotational diffusion in three dimensions is expected for proteins in solution. We assume here that the diffusion is isotropic.

$$\begin{aligned} \Delta F_{\perp}(t) &= a - b e^{-6Dt} - c e^{-20Dt} \\ \Delta F_{\parallel}(t) &= a + 2b e^{-6Dt} - \frac{8}{3} c e^{-20Dt}, \end{aligned} \quad (27)$$

where

$$a \equiv \frac{1}{2}(2 - \eta g_0) \quad (28)$$

$$b \equiv \frac{5}{14} \eta (g_0 - 3g_2) \left(\frac{Z_1 + \frac{7}{3}Z_2}{Z_1 + \frac{10}{3}Z_2 + 5Z_3} \right) \quad (29)$$

$$c \equiv \frac{9}{112} \eta \left(g_0 - 10g_2 + \frac{35}{8}g_4 \right) \left(\frac{Z_1}{Z_1 + \frac{10}{3}Z_2 + 5Z_3} \right), \quad (30)$$

where

$$\eta \equiv \exp(-BX_2). \quad (31)$$

The three-dimensional g_k are products of a Gamma function Γ and an incomplete Gamma function γ^* (Abramowitz and Stegun, 1965, section 6.5) with arguments involving both the wobble angle range and bleaching depth, as follows:

$$g_k \equiv \Gamma\left(\frac{k+1}{2}\right) \gamma^*\left(\frac{k+1}{2}, BX_1\right). \quad (32)$$

Labeled Proteins in Membranes: Random Dipole Orientation with 2-D Rotation

One common case is that of labeled proteins with random dipole orientations rotating about a normal to the membrane. A complete solution for a , b , and c to this case involves complicated integrals over Bessel functions which do not appear to have a closed form and must be found by numerical integration. Nevertheless, this case is intermediate between the 2-D and 3-D cases discussed above, and the results already derived can be utilized. The dipoles on the protein are oriented isotropically in three dimensions. This means that the immediate $t = 0$ postbleach values of $\Delta F_{\parallel,\perp}(0)$ are given exactly by the 3-D case (Eq. 27). But the motion is in 2-D, so the subsequent time dependence will have the exponential factors of 4 and 16 as in the 2-D case (Eq. 20). For experiments in which bleaching depth is moderate, $\Delta F_{\parallel,\perp}(t)$ can be approximated as a single $\exp(-4Dt)$ plus a constant.

Behavior of the Solutions

Unless otherwise noted, the comments here apply to both two-dimensional and three-dimensional cases.

Of some experimental importance is the effect of wobbling on $R(0)$ or $r_b(0)$, because these initial values can be considered to be the amplitude of the "signal" in polarized FPR. Without wobbling, $R(0) = 1/5$ and $r_b(0) = 4/7$ for small bleaching depth. As the wobbling cone angle increases toward isotropicity (i.e., $\psi_1 = 0$ and $\psi_2 \rightarrow 90^\circ$),

then the initial ratios approach their asymptotic values at $t = \infty$; i.e., $R(0) \rightarrow 1$ and $r_b(0) \rightarrow 0$.

Parameters a , b , and c are positive for all ranges of wobble angles. They are normalized so that the prebleach fluorescence equals unity. The relative sizes of the parameters contain two important kinds of information: the fractional completeness of the recovery, and the accuracy to which the time-dependent part of the recovery may be approximated by a single exponential. Although the ratios between the parameters are clearly dependent on wobble angle and bleaching depth, some useful conclusions can be drawn in general. Fig. 1 shows ratios b/a and c/b as functions of bleach depth B (assuming zero wobble) and as functions of wobble angle ψ_2 (assuming $B = 1$ and a fast wobble which fills the solid "volume" of a cone such that $\psi_1 = 0$) for two-dimensional diffusion. Fig. 2 shows the corresponding curves for three-dimensional diffusion.

The fractional recovery (defined as $[b + c]/[a + b + c]$) is $\sim 36\%$ (for 3-D) and $\sim 40\%$ (for 2-D) for shallow bleaches and zero wobble. The fractional recovery steadily decreases with increasing bleach depth or solid wobble cone angle.

Ratio c/b indicates the amount of double, rather than single, exponential nature in $\Delta F_{\parallel,\perp}(t)$. In general, c/b decreases with decreasing bleach depth, approaching zero for very shallow bleaches. For most practical bleach depths (i.e., $B \leq 10$) that are likely to be attained with conven-

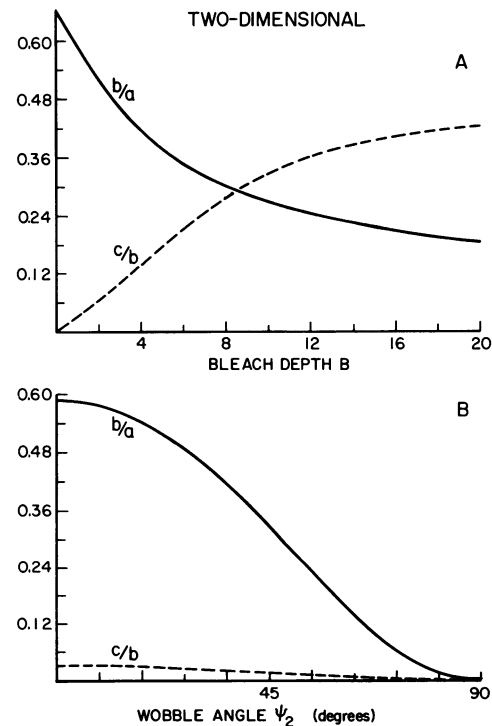


FIGURE 1 Ratio b/a (solid line) and c/b (dashed line), derived from Eqs. 21–23 for two-dimensional diffusion, as functions of (A) bleach depth B , assuming zero wobble (i.e., $\psi_1 = \psi_2 = 0$) and (B) wobble angle ψ_2 , assuming $\psi_1 = 0$ and $B = 1$.

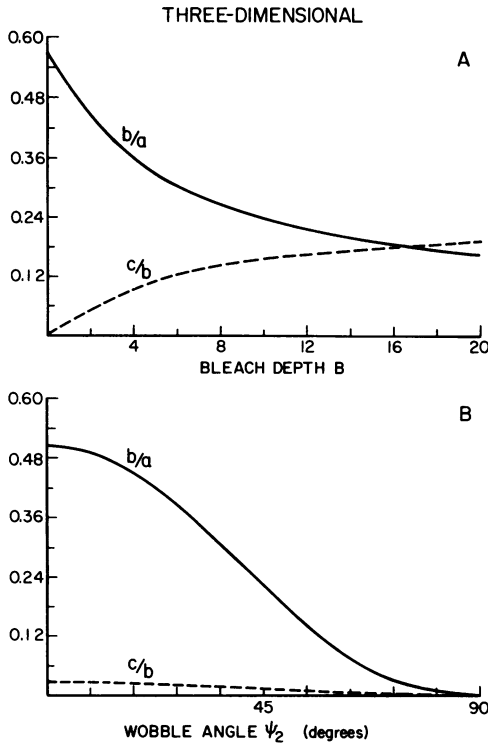


FIGURE 2 Ratio b/a (solid line) and c/b (dashed line), derived from Eqs. 28–30 for three-dimensional diffusion, as functions of (A) bleach depth B , assuming zero wobble (i.e., $\psi_1 = \psi_2 = 0$) and (B) wobble angle ψ_2 , assuming $\psi_1 = 0$ and $B = 1$.

tional lasers while avoiding overheating, $c/b \leq 0.3$ for 2-D diffusion and $c/b \leq 0.16$ for 3-D diffusion. Therefore, for all but the deepest bleaches, a single exponential form is a reasonable quick approximation. Ratio c/b decreases steadily with increasing wobble cone angle for any bleaching depth, making single exponentiality an even better approximation. If we restrict the wobbling to the “walls” rather than the “volume” of a cone (i.e., the polar angle of the wobble motion around its axis is held fixed), ratio c/b goes through a minimum of zero at the “magic” wobble angle of 54.7° . However, the ratio b/a also goes through zero at that fixed “magic” angle, such that no fluorescence recovery occurs at all there.

The fact that c/b remains small for moderate bleach depths also implies that moderate inadvertent prebleaching of a sample due to an overly-long prebleach viewing of the sample or a failure to translate the sample between successive bleaches should have little effect on the characteristic time of the postbleach trace.

The very fast wobbling treated here is only a special case of rotational motions of any speed that may occur during the bleaching pulse. (We restrict the general definition of “wobble,” however, to motions with relaxation times shorter than time scale of the experiment; slower motions directly reshape the fluorescence recovery by introducing a heterogeneity in diffusion coefficient D). The effect of any wobble motions is to change the “initial condition”

imposed on the orientational distribution of bleached fluorophore found immediately after the end of the bleaching pulse. However, the integrations indicated up through Eq. 16 still allow only the $n = 0, 2, 4$ terms to survive. The forms of $R(t)$ and $r_b(t)$ then remain unaltered, always appearing as a ratio of double exponentials with the same two exponents. The only effect of any wobbling theory which performs some sort of weighted integral “average” over the fluorescence lifetime and the bleaching time will be to alter the relative magnitudes of the factors b and c multiplying these exponentials but without changing the exponential rates. Because a general wobbling theory will probably give rise to multipliers b and c intermediate between those for a fast wobbling theory and extremely slow wobbling (i.e., no wobbling at all), we expect that any general wobbling theory will still yield a time course dominated mainly by the slower exponential term for experimentally useable bleach depths. This behavior of the theory should allow a useable measurement of D even if the exact nature of the wobbling is not known.

Multiple Components

If a sample contains multiple noninteracting components with the same bleaching rates but different diffusion coefficients (but all satisfying the assumptions stated at the beginning of the Theory section), then the solutions for $\Delta F_{\perp,1}(t)$ are simply linear combinations of the solutions for each diffusion coefficient D , with factors proportional to the prebleach concentration of each component. If all of the multiple components have the same reversible recovery function $\alpha(t)$, then $R(t)$ and $r_b(t)$ behave monotonically in t (increasing for $R(t)$ and decreasing for $r_b(t)$) regardless of D . But if different components exhibit different $\alpha(t)$ functions, perhaps due to different environments, then the $\alpha(t)$ functions will not cancel in the $R(t)$ and $r_b(t)$ ratios. $R(t)$ and $r_b(t)$ then may no longer be monotonic.

Large Aperture Objectives

As discussed in Axelrod (1979), a high-aperture objective can “look around” the sample. In general, we should write

$$R = \frac{K_a \Delta F_{\perp,1} + K_b \Delta F_{\perp,2} + K_c \Delta F_{\perp,3}}{K_a \Delta F_{\parallel,1} + K_b \Delta F_{\parallel,2} + K_c \Delta F_{\parallel,3}}, \quad (33)$$

where $K_{a,b,c}$ are factors dependent on the half-maximal angle subtended by the objective (Axelrod, 1979), $\Delta F_{\parallel,3}$ and $\Delta F_{\perp,3}$ are given by Eqs. 3 and 4, respectively, and

$$\begin{aligned} \Delta F_{\perp,1}(t) &= \int (\hat{\mu}_a \cdot \hat{z})^2 (\hat{\mu}_c \cdot \hat{x})^2 \Delta C(\Omega, t) d\Omega \\ \Delta F_{\perp,2}(t) &= \int (\hat{\mu}_a \cdot \hat{z})^2 (\hat{\mu}_c \cdot \hat{y})^2 \Delta C(\Omega, t) d\Omega \\ \Delta F_{\perp,1}(t) &= \int (\hat{\mu}_a \cdot \hat{y})^2 (\hat{\mu}_c \cdot \hat{x})^2 \Delta C(\Omega, t) d\Omega \\ \Delta F_{\perp,2}(t) &= \int (\hat{\mu}_a \cdot \hat{y})^2 (\hat{\mu}_c \cdot \hat{z})^2 \Delta C(\Omega, t) d\Omega. \end{aligned} \quad (34)$$

For the objective used in all the experiments described here, a Zeiss 40× water immersion with numerical aperture 0.75, the above correction should amount to < 5% of $R(t)$ at any t , so we will ignore the high-aperture effects.

Fitting Experimental Results to Theory

The purpose of fitting is to derive D from $r_b(t)$ with as few free-fitting parameters as possible. Aside from D , other sets of relevant parameters not known a priori in experimental results include the bleaching depth B , the wobble angles $\psi_{1,2}$, and, for 2-D diffusion only, the tilt angle ϵ , all of which affect the parameters a , b , and c in $r_b(t)$. These variables cannot be ignored in principle; indeed, the relative size of the experimentally observed intercepts $\Delta F_{\parallel,\perp}(0)$ cannot be explained without considering bleaching depth and wobble angles.

Rather than leave a , b , and c to “float” free in a fitting procedure, we employ a much more stringent test which demands that the relative sizes of a , b , and c satisfy the requirements of this theory. Recall that the theory assumes (a) homogeneity and isotropicity in D , (b) homogeneity of spontaneous recovery functions $\alpha(t)$, (c) simple exponential bleaching, and (d) only fast uniform wobbling within the upper and lower cone angle limits $\psi_{1,2}$. Therefore, an inability to attain a good fit would indicate that at least one of these assumptions is not satisfied in our test samples. The fitting procedure used here consists of the following steps (all of which are performed by custom-written MS-FORTRAN programs on a PC-compatible computer).

(a) A nonlinear least squares fitting program (Bevington, 1969), fits the two original $\Delta F_{\parallel,\perp}(t)$ data curves to four-exponential functions with all eight parameters freely floating in each curve. This step smooths the sometimes noisy data while allowing a formally close fit, establishes good values for the intercepts $\Delta F_{\parallel,\perp}(0)$, and allows construction of a smooth $r_b(t)$ according to Eqs. 9 and 10. The fitted parameters themselves are not directly assigned to any physical variable.

(b) According to the theory, each of the intercepts $\Delta F_{\parallel,\perp}(0)$ could arise from a continuous set of complementary wobble angle ranges $\psi_{1,2}$ and bleach depths B . However, for any fixed ψ_1 , the curve described by the complementary values $(\psi_2, B)_{\parallel}$ for $\Delta F_{\parallel}(0)$ will have a unique intersection with the corresponding curve $(\psi_2, B)_{\perp}$ for $\Delta F_{\perp}(0)$. This intersection point, calculated by computer from the theory with the $\Delta F_{\parallel,\perp}(0)$ as input values, indicates a bleaching depth B and a wobble angle ψ_2 consistent with both intercepts. From this information, parameters a , b , and c are computed uniquely (apart from the assumption of some fixed ψ_1).

(c) A nonlinear least squares fitting program fits the theoretical form of $r_b(t)$, Eqs. 9, 10, and 20 or 27, with a , b , and c fixed by step b, to the smoothed experimental $r_b(t)$ derived in step (a). This fit determines the only remaining free parameter, the rotational diffusion coefficient D .

Heating

Signal/noise in polarized FPR (with the signal amplitude defined as $r_b(0)$ and the noise arising from photon statistics) of course improves with bleach depth and probe beam power. A limiting consideration here is sample heating. The following exact integral can be used to calculate numerically the temperature rise $\Delta T(t)$ at any point on the axis of a Gaussian focused laser beam propagating through a three-dimensional light absorbing material. This expression is derived in the same manner as the closed result for dimensional samples discussed in Axelrod (1977), and this expression reduces to the two-dimensional result for thin samples as expected:

$$\Delta T(z, t) = A \int_0^t \tau^{-3/2} d\tau \int_{-\ell}^{-\ell+d} \cdot e^{-\kappa^2/4\mathcal{D}t} (2 + w^2/4\mathcal{D}t)^{-1} d\kappa, \quad (35)$$

where z is the optical axis position at which the temperature is calculated, as measured from the focal plane. The sample of thickness d extends from $z - \ell$ to $z - \ell + d$. The e^{-2} radius w of the Gaussian beam (of semiangle of convergence θ) at any position is related to its radius at the focal plane w_0 by

$$w^2 = w_0^2 + (\kappa + z)^2 \tan^2 \theta. \quad (36)$$

Constant A in Eq. 35 is:

$$A \equiv 1.82 \times 10^{-9} P \epsilon m (4\pi\mathcal{D})^{-3/2}, \quad (37)$$

where $P \equiv$ laser power incident on the sample in watts; $\mathcal{D} \equiv$ heat diffusion coefficient in water = 0.0014 cm²/s; $m \equiv$ number of fluorophores per micrometer cubed; $\epsilon \equiv$ fluorophore extinction coefficient in liters/mole-centimeter.

Comparison with Other Polarization Techniques

We here compare PFPR to time-resolved fluorescence or phosphorescence anisotropy decay (TPA) and to fluorescence depletion anisotropy (FDA). (TPA is an acronym for phosphorescence decay, but its theory is identical to that for any time-resolved luminescence decay technique.)

The theoretical results for PFPR, a “pump-and-probe” technique, are dissimilar to that of TPA, a “pump-only” technique which is limited to faster time scales. Nevertheless, a physical analogy between the two classes of techniques is evident. Both techniques use polarized light flashes to “pump” the system. In the latter technique, a special class of flash-induced fluorophores (excited luminophores) rotate as they decay to their ground state. In the polarized FPR, another special class of luminophores (bleached fluorophores) rotate as they decay to their unbleached state. However, there are two fundamental theoretical differences between the two classes.

(a) The initial conditions corresponding to Eq. 12 have a different dependence on Ω in the two classes of techniques, but this difference approaches zero as the depth of bleaching in PFPR becomes small.

(b) In TPA, postpulse luminescence from pulse-excited molecules is weighted only by the square of the dipole projection along the emission polarizer axis. But in PFPR, the fluorophores are continuously excited by polarized light after the pulse, and this introduces an additional weighting factor of the square of the absorption dipole projection along the probe beam axis.

The similarity between PFPR and FDA (Johnson and Garland, 1981, 1982; Yoshida and Barisas, 1986) is somewhat greater. In both techniques, \perp and \parallel modes refer to the relative polarizations of the pump and probe beams, and both techniques are adapted to a microscope geometry such that the pump and probe beams propagate along the same axis. The only optical difference, in fact, is that Johnson and Garland (1981, 1982) did not employ a microscope polarizing filter through which fluorescence is observed; Yoshida and Barisas (1986) and we employ such a filter for the reason explained previously. Otherwise, fluorescence depletion experiments are exactly like polarized FPR, except that the former are performed on deoxygenated samples to maximize trapping of fluorophores in the triplet excited state after a flash of polarized light. (Such deoxygenation may [Finch et al., 1985] or may not [Damjanovich et al., 1983] affect the mobility of cell membrane components.) Triplet state trapping, which gradually decays back to the ground state, is a form of "reversible bleaching" and indeed may constitute a part of the reversible bleaching we observe on our nondeoxygenated samples.

Therefore, the results of Yoshida and Barisas (1986) for fluorescence depletion are also relevant for PFPR. However, we make certain necessary generalizations in the present work. (a) We allow for arbitrary, rather than small, bleach depths. Practical bleaching parameters may approach $B = 5$, and a general theory is needed to predict the consequent increase in the amplitude of the higher exponential. (b) We allow for wobbling. If wobbling and deep bleaches are neglected, the initial theoretical value of $r_b(0)$ does not ever match the experimental data. (c) We assume a general rather than exponential shape for the reversible recovery $\alpha(t)$, in accordance with observations on our nondeoxygenated samples. (d) We generalize the heating calculation to the actual divergent shape of the focused laser beam rather than approximate it as a cylinder. The latter probably overestimates the temperature increase.

One other distinctive, if less fundamental, feature of the PFPR theory here arises from the optical configuration, here designed for microscopy with an emission analyzer. In some other applications of luminescence polarization for studying molecular orientations and rotations (including

"pump-only," "probe-only," or "pump-and-probe" techniques), the excitation polarization is fixed and the emission polarizer orientation is variable between \parallel and \perp . In this implementation of PFPR, the probe beam and emission polarizer are parallel and the pulse polarization is variable between \parallel and \perp .

A consequence of all of these differences is that the existing theoretical expressions for TPA or FPA do not directly apply to this implementation of PFPR. In particular, consider the two anisotropy expressions $r(t)$ and $r_b(t)$ for TPA and PFPR, respectively. The denominator of $r(t)$, the sum $(F_{\parallel} + 2F_{\perp})$, is used because it is invariant as the excited fluorophores rotate in a sample that is azimuthally symmetric around the excitation polarization direction. For $r_b(t)$, the PFPR analogue of that denominator, $(\Delta F_{\parallel} + 2\Delta F_{\perp})$, is no longer rotationally invariant. (Indeed, no linear combination of $\Delta F_{\parallel, \perp}$ is rotationally invariant with our optical geometry). Another distinction is that $r_b(t)$ never becomes negative, regardless of interdipole angle. Nevertheless, to maintain consistency with the formalisms of Smith et al. (1981), Wegener (1984), and Dale (1987), in which other geometries and polarization schemes are employed, we express our results in terms of $r_b(t)$.

MATERIALS AND METHODS

Sample Preparation

3,3'-dioctadecylindocarbocyanine (diI)-labeled carboxylated latex beads (Seragen Diagnostics, Inc., Indianapolis, IN) were labeled with diI-C₁₈-3 (a gift from A. Waggoner) by incubating 200 μ l of the bead suspension with 10 μ l of a concentrated (0.5 mg/ml) diI/ethanol solution for 15–30 min. The mixture was then passed through a G-75 Sephadex column in Hanks' buffer salt solution (HBSS) to separate unbound diI from the beads. The beads, with diI nonspecifically but tightly adsorbed to their surfaces, came out with the elution volume. They were used the same day and diluted with HBSS to the desired concentration.

For some experiments, the diI-labeled latex beads were encased in Sylgard 182 resin (Dow-Corning) by adding three drops of the bead solution to a 1-ml volume of freshly mixed resin and curing agent, stirring to homogeneity, and allowing the resin to harden at 50°C for several hours.

Covalent binding of RBGT and FBGT to the latex beads was done according to procedure 1 of Dorman (1977). 5 mg of OH-benzotriazole in 0.3 ml of 1:4 dimethylformamide: water was added to 1 ml of the commercial (10% weight solids) aqueous suspension of latex beads. After mixing, the flask was placed in a 5°C cold room in which all subsequent manipulations were performed. Then, 3 mg of 1-ethyl-3-(3-dimethylamino)propyl-carbodiimide hydrochloride (in 0.5 ml of water, prepared just before using) was added dropwise with vigorous stirring. After 6–7 h of stirring in the cold, the sample was dialyzed against 0.1 M NaCl for ~20 h. When removed from dialysis, an excess of FBGT or RBGT solution (Molecular Probes Inc., Junction City, OR) was added until the sample was visibly yellow or pink, respectively. While stirring, we added 0.5 mg of OH-benzotriazole. After stirring 5 d in the cold, the mixture was passed through a G-75-Sephadex column in HBSS to separate any remaining free fluorescent BGT. The labeled latex beads eluted with the void volume. The viscosity was adjusted by diluting the concentrated labeled latex bead suspension with a glycerol-HBSS solution to achieve the desired weight percent of glycerol.

Fetal rat myotube primary cell suspensions were prepared as previously

described (Axelrod et al., 1976b). The medium consisted of 90% Dulbecco's modified Eagle's medium, 10% fetal calf serum, and 0.6 $\mu\text{g/ml}$ tetrodotoxin (TTX, Sigma Chemical Co., St. Louis, MO). At plating time, each 2-ml aliquot of cells in suspension were added to a 35-mm tissue culture dish containing a clean and sterile (but reused) 25-mm-diameter fused silica coverslip (Heraseus-Amersil, Inc., Sayreville, NJ) at a cell count of $\sim 3.5 \times 10^5$ cells/ml. Medium was changed every other day. On days 5–7, the medium was removed and replaced with a solution of fluorescent tetramethyl rhodamine α -bungarotoxin (RBGT, Molecular Probes Inc.) at $\sim 10^{-7}$ M in phosphate-buffered saline (PBS) for 20–30 min at 22°C. RBGT binding is irreversible on the time scale of our experiments. After several washings, the fused quartz coverslip was mounted immersed in PBS containing TTX in a sealed chamber (Bellco Glass Inc., Vineland, NJ).

Optics

Because of the short time scale of some polarized FPR experiments, signal/noise ratio is limited by shot noise, and it is desirable to gather as many photons as possible. In addition, a significant bleaching depth must be achieved with a microsecond-duration bleaching pulse. Therefore, a laser with a power significantly higher than used in conventional FPR is very desirable. We use a 15-W CW argon laser (Coherent Innova Series 20), positioned in our apparatus so that the polarization is horizontal (parallel to the table top).

The optical system is shown in Fig. 3. The laser beam intensity is controlled by an acousto-optic modulator (AOM, IntraAction Corp., Bellwood, IL), the first-order diffraction throughput of which supplies both the bleaching and probe intensities. The AOM can be adjusted so that the ratio of these intensities is $\sim 5,000:1$. The beam then passes through a crystal polarizer oriented horizontally to correct the slight depolarizing effect of the AOM. The beam then passes through a 1/4-wave plate (for $\lambda = 514.5$ nm) and through a transverse field Pockels cells (Lasermetrics Inc., Englewood, NJ). By use of a removable crystal polarizer immediately after the Pockels cell, one can adjust the applied voltages to the Pockels cell such that the output polarization is vertical during a transient pulse (during bleaching in the \perp mode only) and horizontal at all other times. For most experiments, the laser was run at full power (~ 6 W at the laser output for $\lambda = 514.5$ nm) and no other attenuation was employed. The bleaching intensities of the two modes at the sample were confirmed to be within 2% of each other.

The beam passes through a simple converging lens immediately before the entrance field diaphragm of a standard epifluorescence microscope

(Leitz Diavert) illuminator. The converging lens position can be adjusted by an xyz precision translator to set the lateral position and to adjust the spot size at the field diaphragm plane (and correspondingly at the sample plane). The spot was always centered, but it was slightly defocused to avoid overheating the sample while retaining a high total power.

The microscope itself was equipped with a 40 \times , 0.75 NA water immersion achromat objective (Zeiss) and dichroic/barrier filter combinations specially optimized for the $\lambda = 488$ - or 514-nm lines of the source. The illumination spot on the sample had a $1/e^2$ width of 4.1 μm (calculated from the known longitudinal defocus distance at the field diaphragm). After passing through the barrier filter, the fluorescence was repolarized by a film disk (Polaroid) always oriented parallel to the excitation polarization direction of the probe beam. The fluorescence image was delimited by an adjustable image plane diaphragm (part of the Leitz MPV-1 photometer unit), positioned to pass the light from most of the central portion of the illuminated spot. The fluorescence was detected by a high cathode sensitivity, thermoelectrically cooled photomultiplier (RCA C31034A, RCA Electro-Optics, Lancaster, PA).

A standard Merzhäuser microscope stage was custom-modified so that its x and y direction ball slides were driven by high-pitch precision lead screws connected to two computer-driven (and optionally, joystick-driven) microstepping stepper motors (Compumotor Div., Petaluma, CA). The system is capable of making arbitrary-sized position jumps to ± 0.2 μm accuracy.

The heating caused by a bleaching flash can limit the usable range of incident laser powers and focused radii. The temperature increase due to light absorption by the fluorophore can be calculated as discussed in the Theory section. The following optical and sample parameters apply to our experiments on diI/latex beads: $P = 1$ W at $\lambda = 514.5$ nm; $\epsilon = 133,000$; $m = 250$ fluorophores/ μm^3 ; $d = 0.1$ cm; $\ell = 16.9$ μm . The consequent temperature rise at the termination of a 100 μs bleaching pulse is then $\sim 5^\circ\text{C}$. Shorter bleaching pulses produce a smaller temperature increase.

Electronics

An AT-compatible computer (Zenith 241) was central to data acquisition and mechanical and electro-optical control. For data acquisition, the photomultiplier (RCA C31034A) and subsequent pulse discrimination electronics (Ortec Inc., Oak Ridge, TN) supplied photon pulses to a fast photon-counting interface designed and built in our laboratory. This interface contains a buffer which permits short sample times down to 0.5 μs duration, much shorter than available with commercially available PC interfaces. (For sample times longer than 128 μs , however, the pulses are

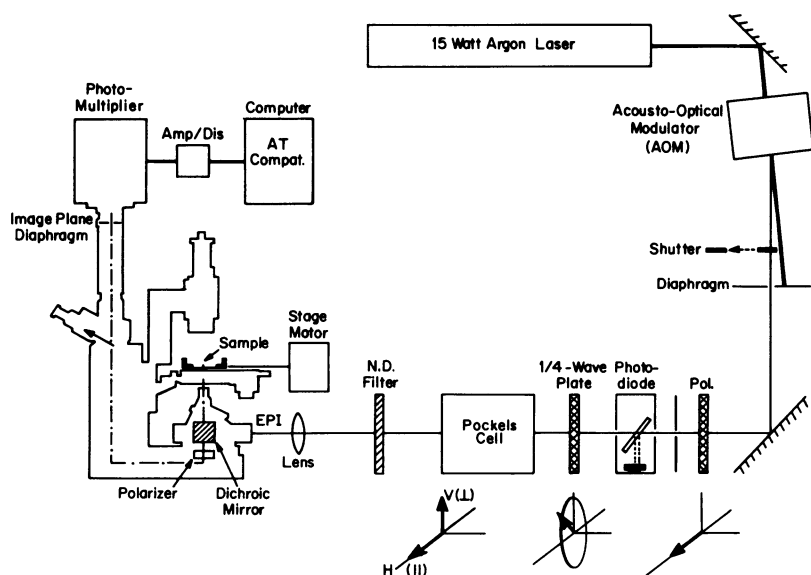


FIGURE 3 Schematic diagram of the optical setup. A detailed explanation is contained in the text. The set of axes near the bottom indicate the polarization of the laser beam as it emerges from the adjacent optical element. The manual shutter is used only to block the light entirely. *Pol.*, crystal polarizer; *N. D.*, optional neutral density filter; *Amp/Dis.*, photon pulse amplifier/discriminator.

automatically routed through a commercial PC counter interface, a Metrabyte CTM-05). A custom-written MS-FORTRAN program accepts the desired experimental parameters related to bleach duration, sample time, number of data points, etc. and translates that information into signals sent to the AOM, to the Pockels Cell, and to the stepper motors. Generally, a 100-point prebleach and 400-point postbleach scan was used, with the bleach duration set equal to one sample time duration.

The fast time scales of polarized FPR require certain technical modifications not used in conventional FPR. We could not use standard glass coverslips to hold the samples because they show a luminescence burst excited by the bleaching pulse that decays with a $\sim 100 \mu\text{s}$ time scale that obscures the experimental data. Fused silica ("quartz") coverslips were used instead. The short sample times also required signal averaging for good signal to noise ratios. To accomplish this in a reasonable amount of time without waiting for translational diffusion to restore fluorescence to its prebleach level at each spot, we use the microstepper motors controlled by the computer to move the microscope stage rapidly in jumps of $\sim 4 \mu\text{m}$ to fresh unbleached spots before each bleaching flash in a rectangular array of user-specified dimensions. The repetition rate was $\sim 10/\text{s}$, so that sufficient dead time was left for damping of jump-induced vibrations.

Fitting Procedure

For most of the experimental data we were able to get a good fit using the stringent procedure described in the theory section. However, in some cases this fit was clearly poor because the smoothed $r_b(t)$ obtained from the four exponential fit of the data showed an anomalous increase immediately after the bleach instead of the expected monotonic decrease. (See the Theory and Discussion sections on the possible origin of this effect). In these cases, those early data points of the F_{\parallel} and the F_{\perp} recovery curves giving rise to the positive sloping region of $r_b(t)$ were deleted. The remaining data points were then subject to the whole fitting procedure described in the Theory section.

In a few cases, this procedure was still too restrictive to yield an acceptable fit. After deleting the initial points as might be required, the rotational diffusion coefficient was obtained by fitting (with a nonlinear least squares program) to a single exponential decay function, corre-

sponding to setting the parameter c in Eqs. 20 or 27 equal to zero and leaving a , b , and D as free-fitted parameters.

EXPERIMENTAL RESULTS

DiI-Latex Beads: Variable Viscosity and Size

To check the feasibility and reliability of PFPR, we obtained D by PFPR for diI-labeled latex beads of various radii and in suspensions of different viscosities. We compare these coefficients to the coefficients calculated from hydrodynamic theory (Saffman and Delbruck, 1975).

Latex beads of $0.175\text{-}\mu\text{m}$ diameter were suspended in glycerol-HBSS of variable viscosities. The results for D , along with relevant fitting parameters, are displayed in Table I. Fig. 4 illustrates a typical set of experimental results for $F_{\parallel,\perp}(t)$ and $r_b(t)$ and their fitted curves. In that particular set, the sample time and bleaching time used was $5 \mu\text{s}$ and the total experimental time to generate a $r_b(t)$ curve was ~ 3 h, and the characteristic time of the decay in $r_b(t)$ is $\sim 800 \mu\text{s}$. Note that the first $165 \mu\text{s}$ (still significantly less than the $800\text{-}\mu\text{s}$ characteristic time) of the trace in Fig. 4 displays an early-time rounding anomaly which is observed on some samples.

Fig. 5, *A* and *B*, show $F_{\parallel,\perp}(t)$ and $r_b(t)$ for a similar sample but with a longer sample time and bleaching time of $25 \mu\text{s}$. In this case, the results show less shot noise because of the longer sample time, and the whole experiment was completed in 1 h. The samples of Figs. 4 and 5, *A* and *B* were separately prepared and not controlled for fluorophore concentration. Note that any early-time anomaly in Fig. 5 *B* is either buried in the noise or absent.

TABLE I
DiI/LATEX BEADS VS. SOLVENT VISCOSITY

A. 0.175 μm							B. 0.327 μm						
Glycerol/H ₂ O	D		No. initial points deleted	B	Wobble angle ψ_2	No. runs	Glycerol/H ₂ O	D		No. initial points deleted	B	Wobble angle ψ_2	No. runs
	Calc	Exp						Calc	Exp				
% (wt/wt)	s^{-1}		<i>Out of 400</i>		<i>Degrees</i>		% (wt/wt)	s^{-1}		<i>Out of 400</i>		<i>Degrees</i>	
0	242	190 ± 24	33	0.90	61	31,000	48	6.8	$3.8 \pm 0.1^*$	0			2,500
	242	164 ± 10	0	2.12	53	10,000							
48	45	$57 \pm 2^*$	15	1.25	66	6,000	56	4.45	$3.4 \pm 0.1^*$	0	2.6	60	3,000
	45	42 ± 1	24	1.17	48	5,000							
56	29	42 ± 1	22	0.91	45	8,000	60	3.5	$1.9 \pm 0.1^*$	0	2.8	69	3,000
	29	$12 \pm 1^*$	33	1.26	46	5,000							
60	23	$17 \pm 1^*$	47	0.96	60	3,000	72	1.34	$1.17 \pm 0.02^*$	0	1.8	33	1,000
	23	$20 \pm 1^*$	42	1.54	62	5,000							
72	9	$7 \pm 1^*$	63	1.32	61	5,000	80	0.62	$0.32 \pm 0.01^*$	0	1.6	65	600
	9	12 ± 1	40	0.77	44	5,000							

This table shows the results for D and the relevant fitting parameters for each experiment. The samples used were either (*A*) $0.175\text{-}\mu\text{m}$ or (*B*) $0.327\text{-}\mu\text{m}$ -diameter diI-labeled latex beads as noted in glycerol/water mixtures with weight percent as noted. The wobble angle ψ_2 (assuming $\psi_1 = 0$) and the bleach parameter B were obtained as described in the text. The calculated D is the value obtained from hydrodynamic theory and the experimental D is the value obtained from the fitted $r_b(t)$ as described in the text. The number of runs refers to each mode (\parallel and \perp). Those experiments fit by single exponentials (i.e., sitting $c = 0$) are noted with an asterisk; all others were fit by the more stringent procedure as described in the text.

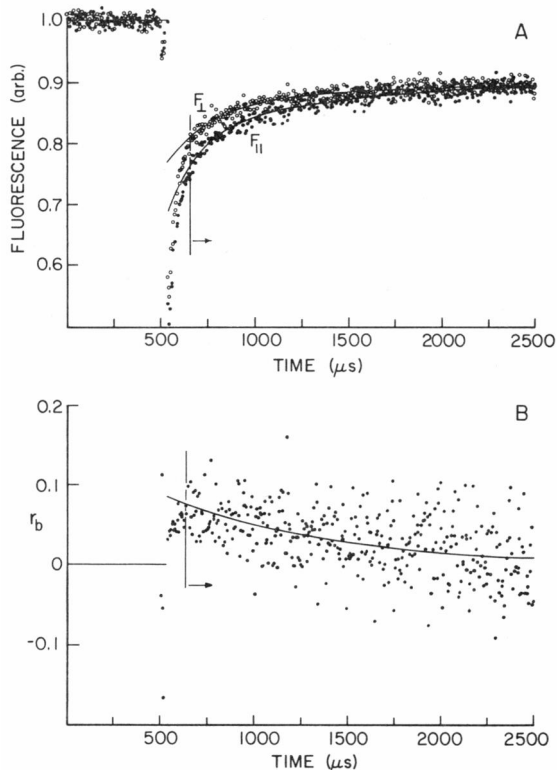


FIGURE 4 Actual polarized FPR data taken on $0.175\ \mu\text{m}$ diameter diI-labeled latex beads in water, with $5\ \mu\text{s}$ sample time. (A) $F_1(t)$ (closed circles) and $F_{\perp}(t)$ (open circles), with corresponding four-exponential fits (solid lines). The ordinate scale is normalized so the mean of the prebleach points in each case is set equal to unity. (B) $r_b(t)$ obtained directly from the data curves (closed circles). Note that these dots are not used for fitting. The fit (solid line) represents a least squares minimization (with D floating) to the $r_b(t)$ ratio formed from the four-exponential fits to the original data $F_1(t)$ and $F_{\perp}(t)$, with a , b , and c determined by the $t = 0$ intercepts of the fits in panel A, as described in the theory section. In this particular set of results, the first 33 data points (left of vertical line) after the bleach were deleted for the fits of both panels A and B, corresponding to the anomalous positive-sloping portion of $r_b(t)$, determined as described in the text.

Nevertheless, the fitting procedure effectively produces reasonable agreement between the diffusion coefficients corresponding to the data of Figs. 4 and 5 B.

Fig. 5, C and D, show analogous results for larger latex beads of $0.327\ \mu\text{m}$ diameter, also with no evident early-time anomaly. This set of results shows the utility of PFPR in a time range clearly much longer than accessible by the triplet-based techniques of TPA and FDA.

Fig. 6, A and B, show the polarized FPR results for D on $0.175\text{-}\mu\text{m}$ -diameter and $0.327\text{-}\mu\text{m}$ -diameter latex beads in suspensions of different viscosities and again compares the results with the predictions of hydrodynamics. The experimental and theoretical results agree reasonably well; in most cases in Fig. 6 A, the discrepancy is $<25\%$. For the larger beads of Fig. 6 B, the experimental data generally follows the theoretical curve but remains below it. This systematic deviation likely reflects some self-aggregation in the sample, which in this sample was visible by eye

through the microscope. According to the manufacturer, surface charge varies with latex sphere size.

When data is collected from samples that show no rotation on the time scale of the experiment, then the anisotropy $r_b(t)$ shows no decay with time. Fig. 7 illustrates two extreme opposite cases. (a) The sample (diI in ethanol) has a rotation time much shorter than the experimental sample time. (b) The sample (diI latex beads encased in hardened Sylgard) is immobilized. In the case of diI in ethanol, $r_b(t)$ has a constant value of zero, as expected. In the other case in which diI/latex beads are immobilized, $r_b(t)$ reaches an expected nonzero asymptote. Note however, that $r_b(t)$ is not constant as expected, but shows an anomalous initial positive slope. The feature is occasionally seen with the other samples and is particularly prominent here. We speculate on the origin of this effect in the Discussion section.

Fig. 8 compares the experimental results for D with those from hydrodynamic theory, as a function of latex bead diameter as reported by the manufacturer. These results for D along with relevant fitting parameters are displayed in Table II. Again, the experimentally measured coefficients are close to the predicted theoretical values.

Rhodamine and Fluorescein on Latex Beads

To determine the feasibility of employing fluorophores commonly used for protein labeling, we obtained D by polarized FPR for latex beads covalently attached with RBGT and FBGT. We compare the results with the corresponding values obtained for the same size diI-labeled beads.

Beads covalently attached with RBGT showed a somewhat different behavior than the diI-labeled ones. The results are displayed in Table III. The rotational diffusion coefficient D was slower than predicted for the particle size used. Nevertheless, D varied inversely with solvent viscosity, as expected from theory. One other feature of these results is useful for interpreting any PFPR data on RBGT: the $r_b(0) = 0.081 \pm 0.002$ value found on this system gives an indication of the maximum r_b likely to be measured on immobilized RBGT.

Beads covalently attached with FBGT showed yet another behavior. We observed an initial very fast decrease of $r_b(t)$ in time, faster than expected for that particle size. The effect persisted at different solvent viscosities and obscured the measurement of the rotational diffusion coefficient.

Acetylcholine Receptor Rotation on Living Myotubes

Rat myotubes in culture present two distinct populations of acetylcholine receptors (AChR): densely clustered receptors, located mainly in regions of contact between the myotube and the culture dish, and nonclustered diffusely

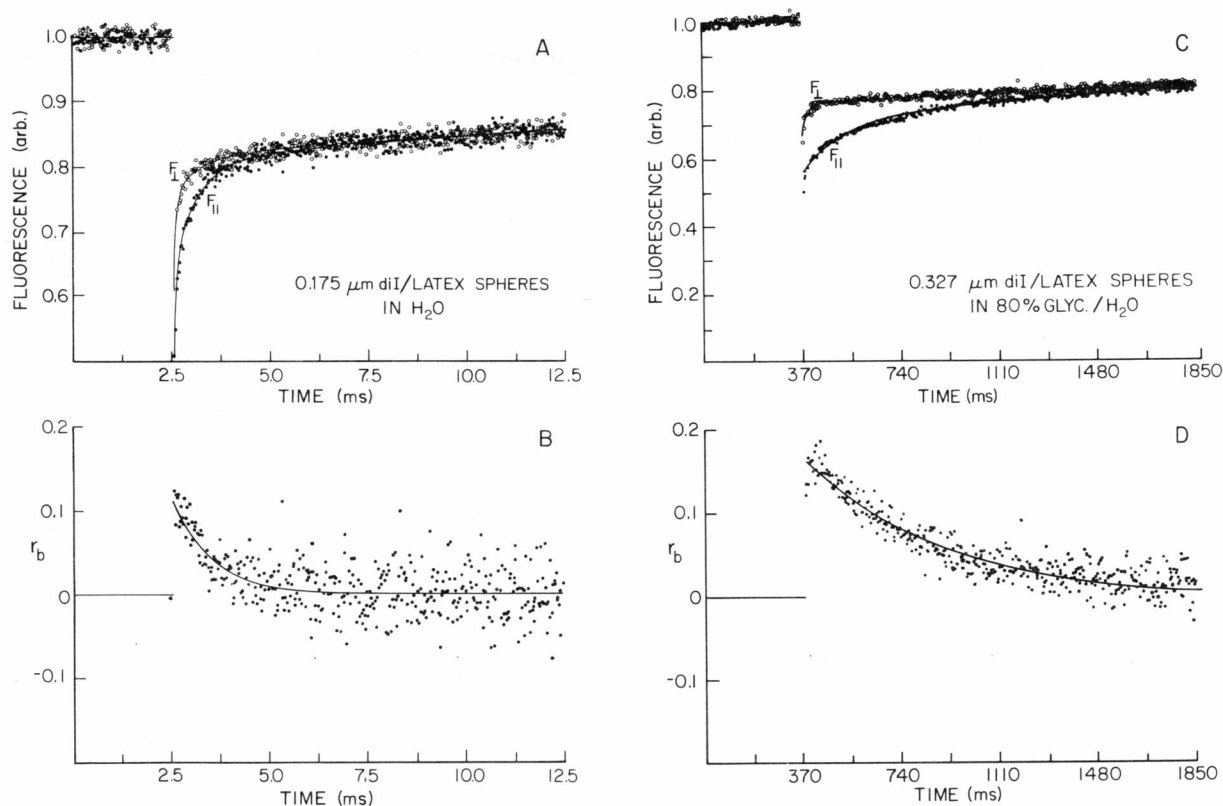


FIGURE 5 (A and B) PFPR data taken on 0.175- μm -diameter diI-labeled latex beads in water, the same type of preparation as for Fig. 4, except with a 25- μs sample time and 25- μs bleaching time here. The data are displayed in the same manner as Fig. 4, except no points needed deletion in the fitting procedure in this case. Although the early-time anomaly noted in Fig. 4 may be buried in the noise of the first six postbleach points here, its presence may be affected by the fluorophore concentration on the beads, which was not well controlled. Number of scans averaged for each polarization, 10,000. (C and D) PFPR data taken on 0.327- μm -diameter diI-labeled latex beads in 80% (wt/wt) glycerol/water, with a sample time and bleaching time of 3,700 μs . This time scale is considerably longer than accessible by triplet probe techniques. No early time anomaly is noted. Number of scans averaged for each polarization, 600.

distributed receptors present all along the surface of the myotubes (Axelrod et al., 1976b)

We performed PFPR experiments on the acetylcholine receptors (marked with RBGT) of living rat myotubes in primary cultures, to measure and compare the rotation of AChR in the two regions. Using the two-dimensional diffusion results presented in the Theory section, we fit the

results according to the protocols as described for the latex bead model systems.

Because the cell's autofluorescence can be a substantial portion (approximately one third) of the diffuse area RBGT-AChR fluorescence, we gathered PFPR data on myotubes whose AChR had been preblocked by an excess of unlabeled α -bungarotoxin before exposure to RBGT.

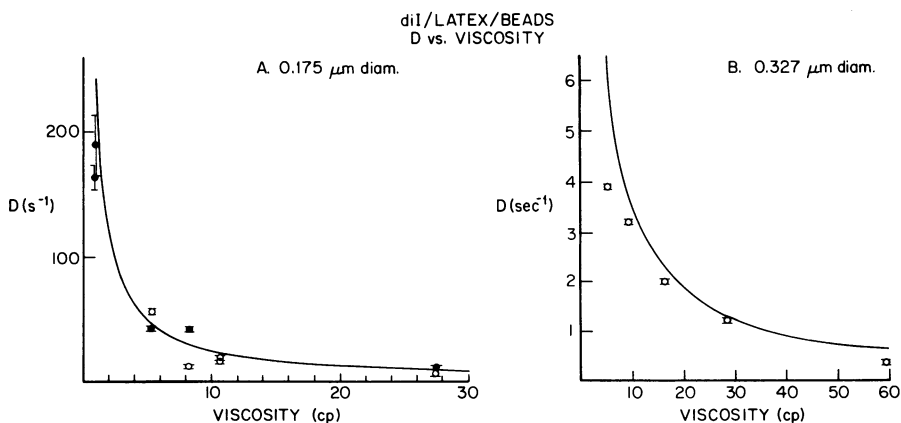


FIGURE 6 Rotational diffusion coefficients D vs. solvent viscosity (in centipoise) for (A) 0.175 μm and (B) 0.327 μm diI/latex beads in glycerol-water mixtures. The values obtained by polarized FPR are shown as points and the theoretical curve from hydrodynamics is a solid line. In those experiments which were repeated twice at a viscosity, both results are presented. Open circles and closed circles represent values obtained from single exponential fits (i.e., setting $c = 0$) and from stringent double exponential fits (with only D floating), respectively.

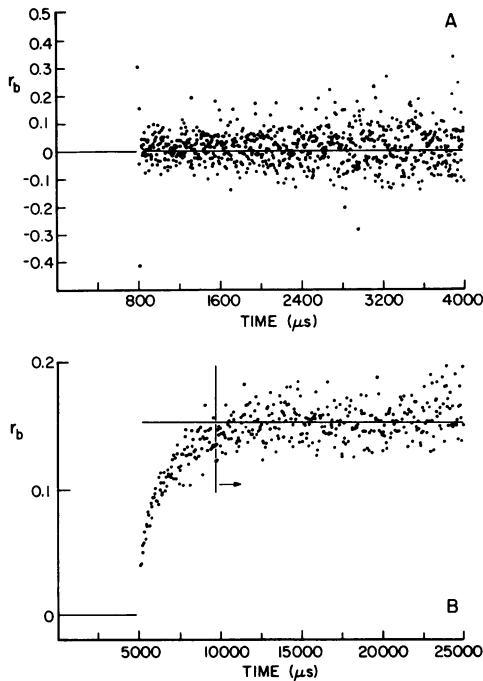


FIGURE 7 $r_b(t)$ for (A) very fast rotating sample (diI in a 70% ethanol solution) and (B) immobile sample (diI-labeled 0.175- μm -diameter latex beads encased in hardened Sylgard). Points to the left of the vertical line in panel B are the early points deleted from fitting procedures as described in text. Note that both fits (solid lines) are flat, as expected for samples with rotational times far out of the range of the experiment. Also note the much longer time scale and the shifted ordinate axis in panel B.

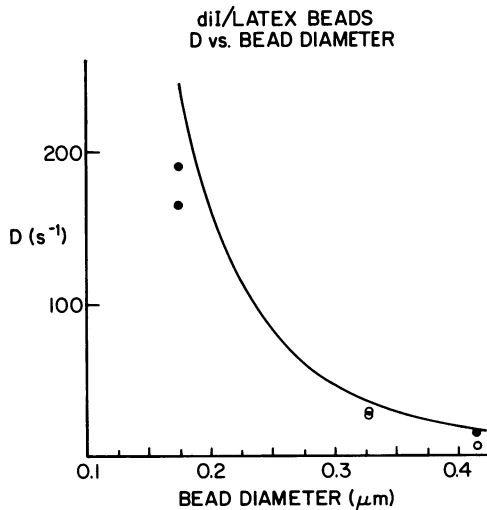


FIGURE 8 Rotational diffusion coefficients D vs. bead diameter for diI/latex beads in water. The values obtained by polarized FPR are shown as points and the theoretical curve from hydrodynamics is a solid line. Experiments were repeated twice for each size and both results are presented. Open circles and closed circles represent values obtained from single exponential fits (i.e., setting $c = 0$) and from stringent double exponential fits (with only D floating), respectively.

TABLE II
DI I/LATEX BEADS IN WATER VS. BEAD DIAMETER

Diameter μm	D		No. initial points deleted	B	Wobble angle ψ_2 Degrees	No. runs
	Calc	Exp				
0.175	242	190 ± 24	33	0.90	61	31,000
	242	164 ± 10	0	1.63	52	10,000
0.327	37	$30 \pm 1^*$	30	1.51	61	10,000
	37	$26 \pm 1^*$	23	1.5	62	7,000
0.415	18	17 ± 1	0	2.6	68	7,000
	18	$7 \pm 1^*$	0	3.05	60	5,000

Fitting details are the same as described in caption of Table I.

These data, in each polarization mode, were routinely subtracted from the respective $F_{\parallel,\perp}(t)$ data taken on labeled myotubes.

The results for $r_b(t)$ on a typical series of experiments are shown in Fig. 9 over several time scales. The diffusely distributed AChR rotate rapidly, with an $r_b(t)$ near zero for all time scales down to 50- μs sample times. However, the clustered AChR show a clearly nonzero $r_b(t)$, indicating that at least a portion of these AChR are rotationally immobile on these same time scales. At the longest time scales shown (800 μs sample time), well out of range of triplet-probe techniques, clustered AChR continue to show immobility.

DISCUSSION

We have shown that polarized FPR is feasible for acquisition and analysis on a variety of samples. For three-dimensional rotational diffusion, we have applied polarized FPR to model systems and were able to measure diffusion coefficients that agreed well with theoretical hydrodynamic expectations. For two-dimensional rotational diffusion, we examined the rotation of an integral membrane protein in nondeoxygenated living cells in culture. The surface concentration of that particular protein (AChR on rat myotubes) is only $\sim 1,000/\mu\text{m}^2$, so we expect that

TABLE III
RBGT/LATEX BEADS, 0.175 μm , VS. SOLVENT VISCOSITY

Glycerol/ H_2O	D		No. initial points deleted	B	Wobble angle ψ_2 Degrees	No. runs
	Calc	Exp				
0	242	$50 \pm 13^*$	10	1.5	55	4,000
	242	70 ± 5	41	0.98	59	20,000
60	23	4 ± 1	38	0.69	64	5,000
	23	7 ± 1	14	0.94	61	5,000

The samples used were 0.175- μm -diameter diI-labeled latex beads in glycerol/water mixtures with weight percent as noted. Fitting details are the same as described in the caption of Table I.

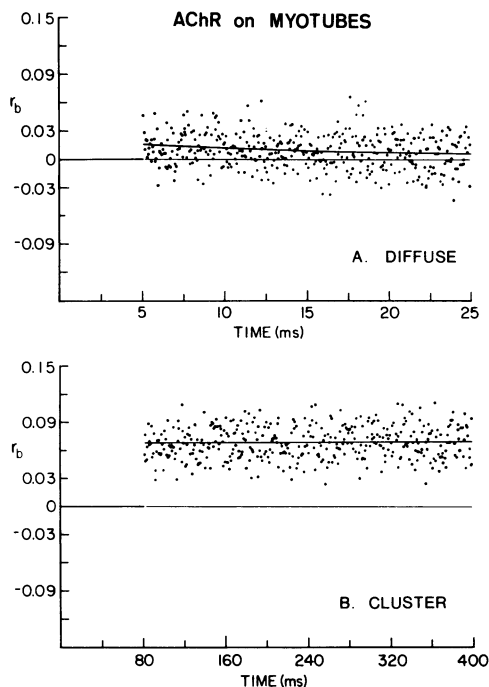


FIGURE 9 $r_b(t)$ of RBGT-labeled AChR on living rat myotubes in primary culture. The dots represent the r_b obtained directly from the data curves. The fits (solid lines) were done as described in the text assuming $c = 0$. (A) AChR in diffuse areas. Sample and bleaching time, 50 μ s. The data presented is an average of $\sim 3,000$ runs (in each mode) obtained from ~ 30 myotubes. The total experimental time, including time for searching the culture dish for target areas, was about 6 h. Although the fit corresponds to a rotational diffusion coefficient of $15 \pm 3 \text{ s}^{-1}$, the low $r_b(0)$ indicates significant rapid rotation even before the first postbleach channel. (B) AChR in cluster areas. Sample and bleaching time, 800 μ s. The data presented is an average of 210 runs from ~ 10 clusters (in each polarization mode). The total experimental time, including searching, was ~ 45 min. The clustered AChR evidently remain immobile within the total postbleach scan time of 0.3 s.

polarized FPR should be feasible for a variety of other cell surface components present at moderate concentrations.

The explicit uncertainty values cited in this paper arise only from photon shot noise and are calculated by standard error propagation techniques. They show that the technique can gather statistically significant data in feasible experimental times. The actual uncertainty in an experiment is likely to arise more from uncertainties in the sample composition itself rather than from inaccuracies in the technique. Such sample uncertainties in our case include self-aggregation of latex beads and biological variability among microscopic regions of cell cultures.

PFPR, as a “pump-and-probe” method, is essentially an extension of fluorescence depletion anisotropy (FDA) in that PFPR applies both to long (> 1 ms characteristic time scales) as well as to shorter time scales limited in principle only by noise from photon statistics. PFPR is mathematically distinct from the “pump-only” methods of time-resolved luminescence anisotropy decay. PFPR has advantages and disadvantages relative to these triplet-based methods. One advantage is its extended applicability to

much longer ranges in which anchored, clustered, or otherwise restricted cell surface proteins might rotationally diffuse; another advantage is that experiments may be performed on normally aerobic and often living samples. A disadvantage is PFPR’s requirement for higher laser power and the consequent attention that must be paid to sample overheating.

The theory here extends beyond that presented for FDA in certain respects. We show explicit results for nonzero interdipole angles, for fast wobbling in a hollow cone of arbitrary wall thickness, and for arbitrary bleach depth, all in a microscope configuration. On the other hand, the theory presented here is more restricted than some others. Wegener (1984) discusses nonmicroscopic optical configurations in which the emission and excitation directions are orthogonal and the polarizer orientations are arbitrary. Yoshida and Barisas (1986) include a discussion of polarized bleaching on spherical samples which should be quite useful for studying suspensions of vesicles; a similar sample configuration could be incorporated into the theory here.

The reversible bleaching present at fast time scales was very conspicuous in all samples with all three fluorophores. The fluorescence spontaneously recovered in nominally immobile samples, on samples with very fast and completely isotropic rotation, and on samples bleached with circularly polarized light. Therefore, the rotational diffusion time is not apparent from the results taken with any single polarization mode and it is essential to take ratios of parallel and perpendicular modes as described in the theory section.

An important conclusion predicted by the theory and confirmed by experiment (as summarized in Tables I, II, and III) is that the calculated rotational diffusion coefficients are rather insensitive to the wobble angle of the fluorophore and to the depth of bleach. Considerable fast wobble occurs on time scales much shorter than the experiment for both covalently and noncovalently anchored fluorophores but it only slightly affects the time course of $r_b(t)$. The wobble mainly reduces the amplitude of the results given by $r_b(0)$, but not beyond the limits of experimental feasibility.

In principle, $r_b(t)$ should be fit to a ratio of double exponentials (the b and c terms of Eqs. 20 or 27) plus a constant a , with the amplitudes and relative rates of each term fixed by theory, and only the diffusion coefficient allowed to float in the fitting procedure. However, because amplitude c is usually small compared with b , the results can be fit to a fair approximation by a ratio of single exponentials plus a constant (i.e., by setting c equal to zero). This implies that the deduction of D is not highly dependent on the assumptions made by the theory. PFPR thereby remains very useable in experimental situations in which the microscopic details of the fluorophore’s interaction with its environment are unknown.

Nevertheless, the theory as presented is exact for arbitrary wobble angle and bleaching depths. Because one of

the objectives of these experiments was to make a strict test of the theory, the results were first fitted very rigorously assuming homogeneity and isotropicity in D , homogeneity of the spontaneous recovery function $\alpha(t)$, simple exponential bleaching, and only fast uniform wobbling within some upper and lower cone angle limits. In some cases, this procedure yielded a very good fit to the data, reflecting the cases in which all the assumptions were probably true.

Other cases showed a deviation from the exact theory. In those instances, the experimental $r_b(t)$ showed an anomalous and short-lived increase during the first points after the bleach rather than showing a monotonic decrease as expected for all postbleach times. This anomaly is apparently not unique to PFPR; it also has been seen by two separate group experimenters with the related FDA technique (Yoshida and Barisas, 1986).

Experimentally, this anomaly occurs when the bleach depths of the \perp and \parallel modes are somewhat similar at $t = 0$ [thereby yielding a small $r_b(0)$] but $F_{\perp}(t)$ subsequently recovers somewhat faster than $F_{\parallel}(t)$. The anomaly could be explained if (a) the sample is heterogeneous in diffusion times or angle or fast wobble, (b) the spontaneous recovery functions $\alpha(t)$ for the various diffusion or wobble components are not identical, and (c) the bleaching efficiencies of the various diffusion components might be different. Under such circumstances, ratios such as $R(t)$ and $r_b(t)$ would not cancel the $\alpha(t)$ spontaneous recovery functions and the monotonicity of the ratios may then be lost.

It is reasonable to suppose that some of our samples contain such heterogeneities. We did not control the concentration of fluorophore bound to each latex bead, the final concentration of beads in the sample, or the extent of self-aggregation. The consequent variability could have given rise to different microenvironments and consequent heterogeneities. The anomalous behavior of $r_b(t)$ varied reproducibly with the bead diameter. According to the manufacturer, each particular size has its own distinctive surface charge density. We noticed that on sample sizes with higher surface charge, the anomalous early-time behavior of $r_b(t)$ was more pronounced. It was most pronounced of all with beads embedded in Sylgard. The apparent heterogeneities of bleaching efficiency, spontaneous recovery rate, and fast wobble angle might be correlated with such variations in microenvironment due to particle charge and surrounding solvent.

The fact that the anomalous behavior of $r_b(t)$ occurred during the first points after the bleach supports the idea that the effect was related to fast reversible bleaching. For fitting purposes only, we deleted the first few data points that lead to the positive initial slope in $r_b(t)$ and based the fits on the remaining points. In this manner, the great majority of points that reflect fluorescence recovery due to rotation of the particles are left unaffected.

The results for D on latex beads depended somewhat on the type of fluorophore coating. RBGT-labeled beads gave a lower than expected diffusion coefficient. It is likely that,

during the labeling procedure, some BGT protein molecules bound more than one bead, thereby causing some aggregation of the particles. The measured D was then somewhat decreased, corresponding to an average over a mixture of aggregates of different sizes. For FBGT, the labeling procedure was the same as for rhodamine α BGT, probably yielding the same sort of aggregation. However, for FBGT, we observed a very rapid initial decrease in $r_b(t)$, followed by a much slower long-time decrease. The early-time feature could arise from $\alpha(t)$ heterogeneities as explained above, but here yielding a decrease instead of an increase. Alternatively, the initial slope could reflect some actual fast diffusion process in the sample, perhaps wobble of the fluorescein on a time scale long enough to alter the shape of $r_b(t)$ rather than merely decrease its $t = 0$ amplitude. Why such wobble would be slower for fluorescein than rhodamine in corresponding series of experiments is not clear. The time scale of the initial rapid decrease of $r_b(t)$ increased in proportion to the viscosity, supporting the notion that the effect arose from an actual diffusive property of the sample. A practical conclusion drawn from this set of experiments is that RBGT and not FBGT is probably better for measuring the rotation of AChR on cell membranes.

The PFPR results for rotational mobility of AChR on cultured myotubes are the first such measurements on living, nondeoxygenated single cells in culture. The PFPR results demonstrate for the first time the nonclustered ("diffuse-area") AChR on nondisrupted living cells are predominately rotationally mobile. Furthermore, the results show that clustered AChR are predominately immobile to times as long as at least 0.3 s. These results extend, to a much longer time scale and to living cells, the TPA observations of Lo et al. (1981) and Bartholdi et al. (1981) that AChR on a (dead) Torpedo membrane fragment preparation are rotationally immobile within at least one millisecond duration. The difference between diffuse-area and clustered AChR with respect to rotational diffusion is analogous to the previously observed difference in lateral diffusion (Axelrod et al., 1976b) for which clustered AChR appear essentially immobile but approximately half of the nonclustered AChR are mobile.

The AChR population in each area may be a mix of mobile and immobile receptors. The proportion f of RBGT/AChR that are rotationally mobile in either area can be estimated from the $r_b(0)$ values in Fig. 9, *A* and *B* in comparison with the maximum possible r_b^{\max} that would be measured if all RBGT fluorophores were mounted on immobile AChR. (Note that the calculation of f is more complex than taking a simple proportion with respect to $r_b^{\max}(0)$ because r_b is a ratio.) Ratio r_b^{\max} is not simply the 4/7 value that would apply were there no fast wobbling; instead, r_b^{\max} may be estimated from the $r_b(0) = 0.081 \pm 0.002$ value obtained from RBGT covalently attached to latex beads in 60% glycerol. Comparing that r_b^{\max} to the $r_b(0) = 0.068 \pm 0.001$ measured on RBGT at AChR

clusters on myotubes and the $r_b(0) = 0.016 \pm 0.002$ measured on RBGT at AChR diffuse areas, one can deduce that the mobile fraction f is 0.20 in cluster areas and 0.83 in diffuse areas.

Although the polarized FPR experiments on myotube AChR are moderately long (1–3 h) for the fastest time scales at the lowest fluorophore surface concentrations, they are feasible with signal averaging and computer-controlled stage motion. Experiments in progress are aimed at how the rotational motion of the AChR is affected by age of culture or by biochemical factors that affect the distribution of the receptors along the surface of the myotubes. Any change in rotational motion would be a sensitive reflection of an interaction of the receptor proteins with either cytoskeletal proteins, extracellular matrix components, or other membrane proteins.

We thank Kate Barald for useful discussions on the myotube experiments and Paul Selvin and Bethe Scalettar for useful discussions on the theory and instrumentation. We are very grateful to Robert Fulbright for his help on the computer software and to Ed Hellen for his help with instrumentation problems. Thanks also to Yvette Dorsey and Sylvia Shiloff for plating the myotube cultures and to Alan Waggoner for his gift of dil.

This work was supported by National Institutes of Health grant NS-14565 to D.A. and National Science Foundation grant PCM-8317271 to Kate Barald of the University of Michigan Department of Anatomy and Cell Biology. M.V. was supported in part by an International Fellowship from the American Association of University Women.

Received for publication 8 September 1987 and in final form 22 December 1987.

REFERENCES

Abramowitz, M., and I. A. Stegun. 1965. Handbook of Mathematical functions. Dover Publications, New York. 1046 pp.

Axelrod, D. 1977. Cell surface heating during fluorescence photobleaching recovery experiments. *Biophys. J.* 18:129–131.

Axelrod, D. 1979. Carbocyanine dye orientation in red cell membrane studied by microscopic fluorescence polarization. *Biophys. J.* 26:557–574.

Axelrod, D. 1983. Lateral motion of membrane proteins and biological function. *J. Membr. Biol.* 75:1–10.

Axelrod, D., D. E. Koppel, J. Schlessinger, E. Elson, and W. W. Webb. 1976a. Mobility measurement by analysis of fluorescence photobleaching recovery kinetics. *Biophys. J.* 16:1055–1069.

Axelrod, D., P. Ravdin, D. E. Koppel, J. Schlessinger, W. W. Webb, E. L. Nelson, and T. R. Podleski. 1976b. Lateral motion of fluorescently

labeled acetylcholine receptors in membranes of developing muscle fibers. *Proc. Natl. Acad. Sci. USA.* 73:4594–4598.

Bartholdi, M., F. J. Barrantes, and T. M. Jovin. 1981. Rotational molecular dynamics of the membrane-bound acetylcholine receptor revealed by phosphorescence spectroscopy. *Eur. J. Biochem.* 54:273–304.

Bevington, P. R. 1969. Data Reduction and Error Analysis for the Physical Sciences. McGraw-Hill Book Co., New York. 336 pp.

Dale, R. E. 1987. Depolarized fluorescence photobleaching recovery. *Eur. Biophys. J.* 14:179–183.

Damjanovich, S., L. Tron, J. Szollösi, R. Zidovetzki, W. L. C. Vaz, F. Regateiro, D. Arndt-Jovin, and T. M. Jovin. 1983. Distribution and mobility of murine histocompatibility H-2^b antigen in the cytoplasmic membrane. *Proc. Natl. Acad. Sci. USA.* 80:5985–5989.

Dorman, L. C. 1977. Method for forming an amide bond between a latex and protein. United States Patent No. 4,045,384.

Finch, S. A. E., H. M. Piper, P. G. Spieckermann, and A. Stier. 1985. Anoxia influences the lateral diffusion of a lipid probe in the plasma membrane of isolated cardiac myocytes. *Basic Res. Cardiol.* 80:149–152.

Jackson, J. D. 1975. Classical Electrodynamics. 2nd ed. John Wiley and Sons, New York. 848 pp.

Jameson, D. M., G. Weber, R. D. Spencer, and G. Mitchell. 1978. Fluorescence polarization: measurements with a photon counting photometer. *Rev. Sci. Instrum.* 49:510–514.

Johnson P., and P. B. Garland. 1981. Depolarization of fluorescence depletion. *FEBS (Fed. Eur. Biochem. Soc.) Lett.* 132:252–256.

Johnson, P., and P. B. Garland. 1982. Fluorescent triplet probes for measuring the rotational diffusion of membrane proteins. *Biochem. J.* 203:313–321.

Kinosita K., S. Kawato, and A. Ikegami. 1977. A theory of fluorescence polarization decay in membranes. *Biophys. J.* 20:289–305.

Kinosita, K., S. Kawato, and A. Ikegami. 1984. Dynamic structure of biological and model membranes: analysis by optical anisotropy decay measurement. *Adv. Biophys.* 17:147–203.

Lo, M. M. S., P. B. Garland, J. Lamprecht, and E. A. Barnard. 1980. Rotational mobility of the membrane-bound acetylcholine receptor of Torpedo electric organ measured by phosphorescence depolarization. *FEBS (Fed. Eur. Biochem. Soc.) Lett.* 111:407–412.

Scalettar, B. A., P. R. Selvin, D. Axelrod, J. E. Hearst, and M. P. Klein. 1988. A fluorescence photobleaching study of the microsecond reorientational motions of DNA. *Biophys. J.* 53:215–226.

Smith, L. M., R. M. Weis, and H. M. McConnell. 1981. Measurement of rotational diffusion in membranes using fluorescence recovery after photobleaching. *Biophys. J.* 36:73–91.

Szabo, A. 1984. Theory of fluorescence depolarization in macromolecules and membranes. *J. Chem. Phys.* 81:15–167.

Wegener, W. A. 1984. Fluorescence recovery spectroscopy as a probe of slow rotational motions. *Biophys. J.* 46:795–803.

Wegener, W. A., and R. Rigler. 1984. Separation of translational and rotational contributions in solution studies using fluorescence photobleaching recovery. *Biophys. J.* 46:787–793.

Yoshida, T. M., and B. G. Barisas. 1986. Protein rotational motion in solution measured by polarized fluorescence depletion. *Biophys. J.* 50:41–53.